Measurements in Wall Turbulence

by

Sidqi A. Abu-Khamsin

A Thesis Presented to the

FACULTY OF THE COLLEGE OF GRADUATE STUDIES

KING FAHD UNIVERSITY OF PETROLEUM & MINERALS

DHAHRAN, SAUDI ARABIA

In Partial Fulfillment of the
Requirements for the Degree of

MASTER OF SCIENCE

In

CHEMICAL ENGINEERING

December, 1977

Order Number 1355700

Measurements on wall turbulence

Abu-Khamsin, Sidqi A., M.S.

King Fahd University of Petroleum and Minerals (Saudi Arabia), 1977

U·M·I
300 N. Zeeb Rd.
Ann Arbor, MI 48106

MEASURMENTS ON WALL TURBULENCE

by

SIDQI A. ABU-KHAMSIN

A Thesis Presented to the

FACULTY OF THE GRADUATE SCHOOL

UNIVERSITY OF PETROLEUM & MINERALS

DHAHRAN, SAUDI ARABIA

In Partial Fulfillment of the

Requirements for the Degree of

MASTER OF SCIENCE IN CHEMICAL ENGINEERING

December, 1977

UNIVERSITY OF PETROLEUM & MINERALS

DHAHRAN, SAUDI ARABIA

THE GRADUATE SCHOOL

This thesis, written by

MR. SIDQI A. ABU-KHAMSIN

under the direction of his Thesis Committee, and approved by all its members, has been presented to and accepted by the Dean of the Graduate School, in partial fulfilment of the requirements for the degree of

MASTER OF SCIENCE IN CHEMICAL ENGINEERING

Fahd H. Oakhil
Dean of the Graduate School

Date 12/15/77

Fahad A. Smait
Department Chairman

Thesis Committee

Edward W Comings
Chairman

M. Sami Selim
Member

Member

Member

This Thesis is dedicated to MONA

ACKNOWLEDGMENT

Acknowledgment is due to the University of Petroleum and Minerals for support of this research.

I wish to express my deep appreciation to Professor Lindon C. Thomas who served as my thesis advisor, and whose help, direction and encouragment made this work an enjoyable experience and a possible achievement. I also wish to thank Dr. E.W. Comings, the comittee chairman, for his help in the construction of the wind tunnel and for his valuable suggestions and directions. Acknowledgment is also due to the other members of the committee, Dr. M. Sami Selim and Dr. Saad El-Sherbiny.

TABLE OF CONTENTS

	Page
LIST OF TABLES	v
LIST OF FIGURES	vi
ABSTRACT	1
INTRODUCTION	2
LITERATURE SURVEY	3
Experimental Evidence	3
Theoretical Formulations	9
EQUIPMENT AND PROCEDURES	15
Flow System	15
Measuring Equipment	18
Hot-Wire Equipment	18
Recording Equipment	19
Velocity Measuring Equipment	19
Procedures	22
Test Runs	22
Data and Data Treatment	23
RESULTS, DISCUSSION AND CONCLUSIONS	30
Boundary Layer Measurements	30
Conclusions	40
Recommendations For Further Work	41
NOMENCLATURE	42
REFERENCES	44

LIST OF TABLES

Table		Page
I	Raw and Calculated Data for Test Run # 1	27
II	Raw and Calculated Data for Test Run # 2	29

LIST OF FIGURES

Figure		Page
1	Flow System	16
2	Wind Tunnel	17
3	Probe-Traversing-Mechanism System	20
4	Probe-Plate Contact Point	21
5	Sample Photographed Signals	24
6	Interpretation of a Typical Signal	26
7	Normalized Pressure Gradient Parameter K vs. Boundary Layer Reynolds Number Re_x for Test Run # 1	32
8	Mean Burst Period vs. Re_x for Test Runs # 1 and 2	33
9	Comparison of Mean Burst Period of Test Run # 1 with Theory and Literature Data	35
10	Comparison of Mean Burst Period of Test Run # 2 with Theory and Literature Data	36
11	Summary of Literature Data	37

ABSTRACT

Hot-wire anemometry techniques were used to investigate wall turbulence for boundary layer flow over a flat plate. The anemometer signals were visually analysed to obtain the frequency of occurence of the burst process. Both fully turbulent and transitional turbulent flows were studied with emphasis placed on the later. It was observed that the burst period, measured at a point off the wall, increases to infinity as the Reynolds number decreases and approaches laminar conditions. The results obtained are in basic agreement with off-wall literature data for fully turbulent flow. As for the transitional region data, no literature data are available for comparison.

INTRODUCTION

The wall region in turbulent flow fields gains its importance from the simple fact that all the mass and energy exchange processes between the flow and its boundaries take place within this region. The hydrodynamic character of the flow near the wall greatly affects these transport processes.

While the laminar boundary layer problem has been completely investigated and modelled, the turbulent boundary layer is still not thoroughly understood. Several theories approaching the problem from different modelling concepts have been proposed. One of the most recent of these is the surface renewal approach. This approach is based on the observed unsteady transport processes associated with it.

The main objective of this study is to experimentally investigate this feature of wall turbulence. The working plan will be to a) design and construct a wind tunnel of average dimensions and performance, and b) obtain preliminary measurments on the frequency of wall turbulence for boundary layer flow, with emphasis placed on transitional turbulent flow.

LITERATURE SURVEY

EXPERIMENTAL EVIDENCE

Experimental observations of the behavior of the wall region in turbulent flow fields have consistently reflected the unsteady nature of this region. The earliest of these studies included Fage and Townend (1) and Lin, Moulton and Putnam (2). In recent years, the nature and structure of the flow in this region have been the subject of extensive research work. As a consequence of these experimental studies of wall turbulence, Danckwerts (3) developed the surface renewal modeling concept. Based on this approach, fluid in the wall region is assumed to be periodically renewed by fresh fluid from the turbulent core.

One of the earliest experiments which revealed some quantitative information pertaining to the period of renewal was the work of Einstein and Li (10). Having noticed the mixing of a dye injected in the viscous sublayer of a smooth boundary layer flow with the material further removed from the wall, they proposed their surface renewal based model of the periodically growing and disintegrating sublayer. With oil flowing in a one-foot wide channel at a velocity of 6.27 fps, the wall pressure fluctuations sensed by a pressure transducer were recorded and correlated. A mean period of boundary layer growth and decay was clearly

observed. However, they could not give a reasonable explanation for the generation of new turbulence and the transmission of shear from this unsteady sublayer to the turbulent flow.

The development of high frequency response transducers, hot-wire anemometers and other supplementary high precision electronic and mechanical devices have facilitated the ability to obtain more accurate quantitative information on the frequency of turbulence. A good amount of data has been collected during the last fifteen years. A summary of some of the important experimental studies on this subject is given below.

Kline, Reynolds, Schraub and Runstadler (The Stanford Group) (11) studied turbulent boundary layers employing both visual and hot-wire anemometry techniques. Performing their experiments in a close circuit water flow set-up with two test channels of different dimensions, their studies revealed the presence of various dependent motions within the viscous sublayer of the flow. They described these motions and their interaction with the outer flow as the burst phenomena. The burst cycle was reported to consist of lift-up, oscillation, bursting and ejection processes.

Different flow conditions were imposed with pressure gradients varying from strongly adverse to strongly favorable values. Traditional hot-wire anemometer traverses were carried out in the viscous sublayer very close to the wall ($y^+ = 0.2$) coupled with two visual methods wall-slot dye injection and hydrogen bubble techniques. In the first method, a dye was injected over the wall bounding the flow

and the behavior of the dye streams was studied. In the other method, very small hydrogen bubbles were generated in streams within the flow by electrolysis of water with an electrolysis cell. The local velocity profiles and their development for all types of flows were determined from the analysis of photographs obtained from still and moving cameras. Measurments were made close to the wall at $y^+ = 0.15$ for the bubble technique and $y^+ = 0$ for the dye technique. The visually measured burst periods were in excellent agreement with the ones obtained from short sample time autocorrelations.

The next step was to determine the rate at which the burst process took place. This was done by simply counting the rate of break up of the dye or hydrogen bubble streaks per unit of span. Plots of the burst rate F versus the friction velocity u^* ($= u_\infty \sqrt{f_x/2}$) were prepared. An important observed feature was the dependence of the normalized burst rate $F^+ (=F\nu^2/u^{*3})$ on K $(-\nu^2/(\rho u_\infty^3)dP/dx)$, a dimensionless pressure gradient parameter, and the disappearance of bursts when K exceeded 3.7×10^{-6}. This means that bursting ceased at a certain pressure gradient which confirms the observations of Kays and Moretti (19) of relaminarization of turbulent boundary layers.

One of the most sophisticated experimental set-ups to investigate the turbulent boundary layer was the one developed by Corino and Brodkey (12). Their equipment was designed to make possible a visual analysis of the flow without introducing elements that would disturb it. Their carefully designed close circuit flow system was equipped with a high speed motion picture camera

which moved with the flow at various preset speeds. Very fine magnesium oxide particles, which served as tracers as they reflected light, were suspended in the flow medium, trichloroethylene.

Their experimental observations of the various events taking place within the viscous sublayer of the flow $y^+ < 40$ revealed the existance of various types of motions. They observed periodic ejections of fluid elements from the sublayer to the turbulent core of the flow. This ejection process, mostly within the region $5<y^+<15$, was observed to always be preceeded by a certain sequence of events. The sequence was initiated by deceleration of fluid layers near the wall. Then these layers were reaccelerated by influx of fluid from the main stream. A region of high shear was then created which led to fluid element ejection. The ejection process was first detected at Re = 5360 (pipe flow) and continued with the same sequence and character as the Reynolds number was increased, but with increased intensity and frequency of occurence and with greater impact on the turbulence of the flow.

Corino and Brodkey summarized their observations by dividing the wall region into three rather distinct regions. The region of $y^+< 5$ was not laminar but was still disturbed by velocity fluctuations of small magnitude and penetration of fluid elements from the outer layers. The most important feature of wall region turbulence occured in the region $5<y^+<70$ where fluid element ejections were reported to possess a well defined nature which was independent of the mean flow parameters. Also, the interaction of the ejection processes with the main flow was the direct cause of turbulence generation. The position of

interaction of these elements with the main flow was $7<y^+<30$. The region beyond $y^+>70$, the turbulent core, was characterized by less intense velocity fluctuations but a larger scale of turbulence.

Meek and Baer (13) conducted fluid flow and heat transfer experiments using air and tetralin flow systems. For both systems, data were collected from platinum film resistance elements fired onto the inner walls of glass tube test sections of different diameters. A high sensitivity, high frequency response pressure transducer and a boundary layer probe were employed in the air system for additional data. Signals from the platinum sensors were subjected to spectral analysis and correlation and the mean period $1/\bar{s}$ of the lift-up process was determined. Their results showed a constant dimensionless period $u^* \sqrt{1/(\nu \bar{s})} \simeq 15$ over a range of Reynolds numbers from 5×10^3 to 2×10^5 for air; and $u^* \sqrt{1/(\nu \bar{s})} \simeq 20$ over a shorter range of Reynolds numbers for tetralin. Calculations for $1/\bar{s}$ based on their theoretical surface renewal model, which was a modification of the Einstein and Li's (10) were in basic agreement with a value of $u^* \sqrt{1/(\nu \bar{s})} \simeq 17$.

Strickland and Simpson (18) studied turbulent boundary layer separation in a wind tunnel. Their measurements of fluctuating wall shear stress and burst frequency were obtained by both hot-film and laser anemometry. Of particular interest to us are their measurments on zero pressure gradient flows. Information pertaining to the burst frequencies was extracted from analysis of the distribution curves of the power spectral density function of the wall shear stress fluctuations for several flows. Both wall and boundary layer measurments by a flush mounted probe were taken into consideration. Good agreement was obtained between their spectra

data and correlation data by Rao et al. (17). Upon comparison of their burst rate data with other investigators' data, all normalized on outer flow variables, there was considerable agreement as all the data clustered on straight lines.

The work of Thomas and Min (15) gains its importance because of the little information available for the transitional turbulent region. They studied transitional turbulent pulsatile flow in a channel. Using an aqueous saline solution system, they measured the burst frequency in the wall region for different pulse frequencies and flow conditions, e.g., laminar-transitional and fully turbulent flows. With a pressure transducer, a flowmeter and a flush mounted anemometer probe, the unsteady friction factor f(t) and the unsteady burst frequency s(t) were determined. The burst frequency was obtained by visual analysis of the anemometer recorded signal and by autocorrelation of the same signal. The results of the two methods were found to be approximatly the same. Thomas and Min also compared values obtained for the friction factor and the shear stress with surface renewal based predictions and found good agreement. However, their assumption of quasi-steady state conditions appeared to apply only for low pulse frequencies. Finally, they achieved good agreement between their experimental measurments for s(t) by both methods and their surface renewal based calculations in both turbulent flow and transition from laminar to turbulent flow conditions.

As a closure to this survey of experimental work, one can notice the important role of visual analysis techniques in determining burst rate data.

THEORETICAL FORMULATIONS

Danckwerts (3), in his 1951 investigation of the absorption of gases into agitated fluids, questioned the conventional assumption of the existance of a stagnant fluid film through which mass transfer takes place. He assumed that, under conditions where the liquid film controled the transfer rate, this film was continuously renewed with bulk flow material. He envisioned the liquid layers in the interface region as consisting of "a mosaic of elements which have been exposed to the gas for different lengths of time, and which are themselves in due course replaced by fresh liquid having the local average bulk concentration of dissolved gas".

As a consequence of his investigation and the experimental studies of wall turbulence, Danckwerts (3) developed the surface renewal modeling concept. His first attempt to apply this surface renewal and penetration theory was to model a mass transfer system in which the transfer process, neglecting convective mass transfer terms, is represented by the equation:

$$\partial c/\partial \theta = D(\partial^2 c/\partial y^2) \qquad (1)$$

and the boundary conditions:

$$c = C_i \ , \ y > 0 \ , \ \theta = 0 \qquad (2)$$

$$c = C_o \ , \ y = 0 \ , \ \theta > 0 \qquad (3)$$

$$c = C_i \ , \ y = \infty \ , \ \theta > 0 \qquad (4)$$

Where θ is the time elapsed from the beginning of the surface renewal cycle. C_o and C_i are the equilibrium concentration and the initial concentration of the flow, respectively. The second boundary condition indicates that the concentration of the flow in the interface region assumes the equilibrium value

throughout the renewal process. The renewal process is so rapid that the fluid element can be regarded as a semi-infinite medium relative to the solid boundary. This is reflected in the third boundary condition where the concentration within the fluid element remains equal to its initial concentration C_i during the renewal process. The solution for the unsteady concentration profile is thus,

$$c = C_i + (C_o - C_i) \operatorname{erfc} [y/(2\sqrt{D\,\theta})] \tag{5}$$

and the instantaneous transfer rate is,

$$R(\theta) = -D(\partial c/\partial y)_{|y=0}$$

$$= (C_o - C_i)\sqrt{D/(\pi\theta)} \tag{6}$$

At this stage, Danckwerts defined the statistical age distribution function $\phi(\theta)$ for the fluid elements at the interface where the fraction of the surface which has been exposed for times between θ and $\theta+d\theta$ is given by $\phi(\theta)d\theta$. Danckwerts further assumed that the renewal process occurs randomly, and hence he utilized the random distribution

$$\phi(\theta) = s \exp(-s\theta) \tag{7}$$

where s is the mean frequency of renewal of liquid surface. If the instantaneous rate of absorption of gas per unit area into an element of surface which has been exposed to gas is designated by $R(\theta)$, the average rate of absorption per unit area of wetted surface will be:

$$\overline{R} = \int_0^\infty \phi(\theta)\ R(\theta)\ d\theta \tag{8}$$

Applying this result to the mass transfer system, the following solution for the average transfer rate is obtained:

$$\bar{R} = (C_o - C_i)\, s \int_o^\infty \sqrt{D/(\pi\theta)}\ \exp(-s\theta)\ d\theta$$
$$= (C_o - C_i)\sqrt{Ds} \qquad (9)$$

The quantity s has to be determined experimentally utilizing data on average transfer rates and concentration differences. However, it has to be emphasized at this point that s is a hydrodynamic parameter and that it emerges as a result of the various hydrodynamic processes which coexist within the flow field. Danckwerts assumed that the mean frequency of renewal is identical for systems of identical conditions, e.g. equal Reynolds numbers and packing parameters.

In 1951, Hanratty (9) and Einstein and Li (10) independently applied Danckwerts' model to calculate the velocity profiles and the wall shear stress in turbulent tube and boundary layer flow fields. The momentum for both of these processes was represented by

$$\partial u/\partial\theta = \nu(\partial^2 u/\partial y^2) \qquad (10)$$

with the initial-boundary conditions

$$u = 0\ ,\ y = 0 \qquad (11)$$
$$u = U_i,\ y = \infty \qquad (12)$$
$$u = U_i,\ \theta = 0 \qquad (13)$$

where U_i is the velocity of the fluid element at the first instant of renewal. The solution for the velocity profile is

$$u = U_i\ \operatorname{erf}\left(y/(2\sqrt{\nu\theta})\right) \qquad (14)$$

and the instantaneous shear stress

$$\tau_o = \rho U_i \sqrt{\nu/(\pi\theta)} \qquad (15)$$

Assuming that all fluid masses have equal residence times of (1/s), the probability of residence time between θ and $\theta+d\theta$ is s. Thus the velocity profile and the shear stress averaged over the whole renewal period are

$$\bar{u} = sU_i \int_0^{1/s} \text{erf}\,(y/(2\sqrt{\nu\theta}))\, d\theta \qquad (16)$$

and

$$\tau_o = s \int_0^{1/s} U_i\sqrt{\nu/(\pi\theta)}\, d\theta = 2\rho U_i\sqrt{\nu s/\pi} \qquad (17)$$

In order to define the initial velocity U_i, Einstein and Li and Hanratty set U_i/u^* equal to empirical constants, where the friction velocity u^* is defined by $u^*=\sqrt{\tau_o/\rho}$. The assumption of uniform residence times is physically unrealistic due to the random nature of the fluid eddy movements. However, Hanratty showed that the form of the probability function had little influence on the calculated profiles.

Meek and Baer (13) obtained a value for U_i by interfacing the surface renewal predictions for $\bar{u}$ with the logarithmic velocity distribution given by

$$u^+ = \bar{u}/u^* = c + 1/\kappa \ln y^+ \qquad (18)$$

Their predictions for the renewal rate s were in fairly good agreement with their experimental anemometer measurements.

Thomas (16) suggested that U_i be approximated by the free stream velocity u_∞ for boundary layer flow and by the bulk velocity U_b for channel and tube flows. His solutions for the temperature profiles for low and moderate Prandtl number fluids, based on the above assumption, correlated the experimental data to a good extent.

Thomas and Kakarala (14) extended surface renewal modeling to hydrodynamically fully developed transitional channel flow. They modeled the unsteady momentum transfer process associated with the surface renewal process by

$$\partial u/\partial\theta = \nu\, \partial^2 u/\partial y - 1/\rho\ \partial P/\partial X \tag{19}$$

where

$$v = \partial u/\partial x = 0 \tag{20}$$

with initial-boundary conditions

$$u = U_b \quad \text{when} \quad \theta = 0 \tag{21}$$

$$u = 0 \quad \text{at} \quad y = 0 \tag{22}$$

$$u = 0 \quad \text{at} \quad y = w \tag{23}$$

where w is the width of the channel. Employing Danckwerts' probability distribution function, the velocity profile and the pressure gradient were transformed into the mean domain; i.e.,

$$\bar{u} = \int_0^\infty u(\theta)\ \phi(\theta) d\theta \tag{24}$$

and

$$d\bar{P}/dx = \int_0^\infty \partial P(\theta)/\partial x\ \phi(\theta)\ d\theta \tag{25}$$

Thus the equation of motion becomes

$$s(\bar{u} - U_b) = \nu\ d^2\bar{u}/dy^2 - 1/\rho\ \ d\bar{P}/dx \tag{26}$$

The solution is

$$\bar{u} = [U_b - 1/(\rho s) d\bar{P}/dx]\ [1 - \cosh(Y/(ws^+))/\cosh(1/(2bk))] \tag{27}$$

where

$$s^+ = \sqrt{\nu/s}/w \tag{28}$$

and

$$Y = w/2 - y \tag{29}$$

and the mean wall shear stress is

$$\tau_o = -\mu \, d\bar{u}/dy|_{\pm w/2}$$

$$= \mu/(ws^+) \tanh (1/(2s^+)) [U_b - 1/(\rho s) \; d\bar{P}/dx] \qquad (30)$$

It can be shown that equations (27) and (30) reduce to the laminar solution of the problem and to the simple surface renewal solution for fully developed turbulent flow as s approaches zero and infinity, respectively. Introducing the Fanning friction factor f, equation (30) is rewritten to be

$$1/(Re\ f) = s^+/2 \, [1/2 \coth(1/(2s^+)) - s^+] \qquad (31)$$

When the empirical formula for the friction factor

$$f = 0.079 \, Re^{-0.25} \qquad (32)$$

was used, equation (31) correlated the experimental data well. Also predictions for the velocity profiles by equation (27) represented the data extremely well in the region of $y^+ < 30$. When equation (31) was applied to predict the surface renewal rate for transitional turbulent quasi-steady pulsatile channel flow, with time dependent parameters, Thomas and Min (15) obtained good agreement with their experimental data.

EQUIPMENT AND PROCEDURES

FLOW SYSTEM

The flow system used in this investigation is a medium-size open circuit wind tunnel. The system is shown schematically in Figure 1. Figure 2 shows a photograph of the wind tunnel. The tunnel is made of plywood sheets except the reducer which is made of galvanized iron sheets and the test section is made of plexiglass with a wooden frame work. The tunnel is mounted on two separate dollies and is 4.42 meters in total length. The several components of the tunnel are described in this section.

1. Blower

   The blower is a centrifugal sirocco-type fan driven by a 1/3 Hp. electric motor. It has a 21.6 cm X 21.6 cm discharge outlet and supplies air at an approximate rate of 35466 liter/min. at full suction capacity. The flowrate can be varied by blocking appropriate sections of the blower suction opening. The blower was mounted on a separate platform to eliminate vibration.

2. First Diffuser

   The first diffuser is 76.2 cm long. Its square inlet and outlet have heights of 18 cm and 61 cm, respectively. Its angle of divergence is 15.8 degrees and the aspect ratio is 1:11.76. Two sets of five vanes are fitted inside the diffuser to distribute the flow uniformly over the cross section. The diffuser was connected to the blower via a rubber tube 25 cm long.

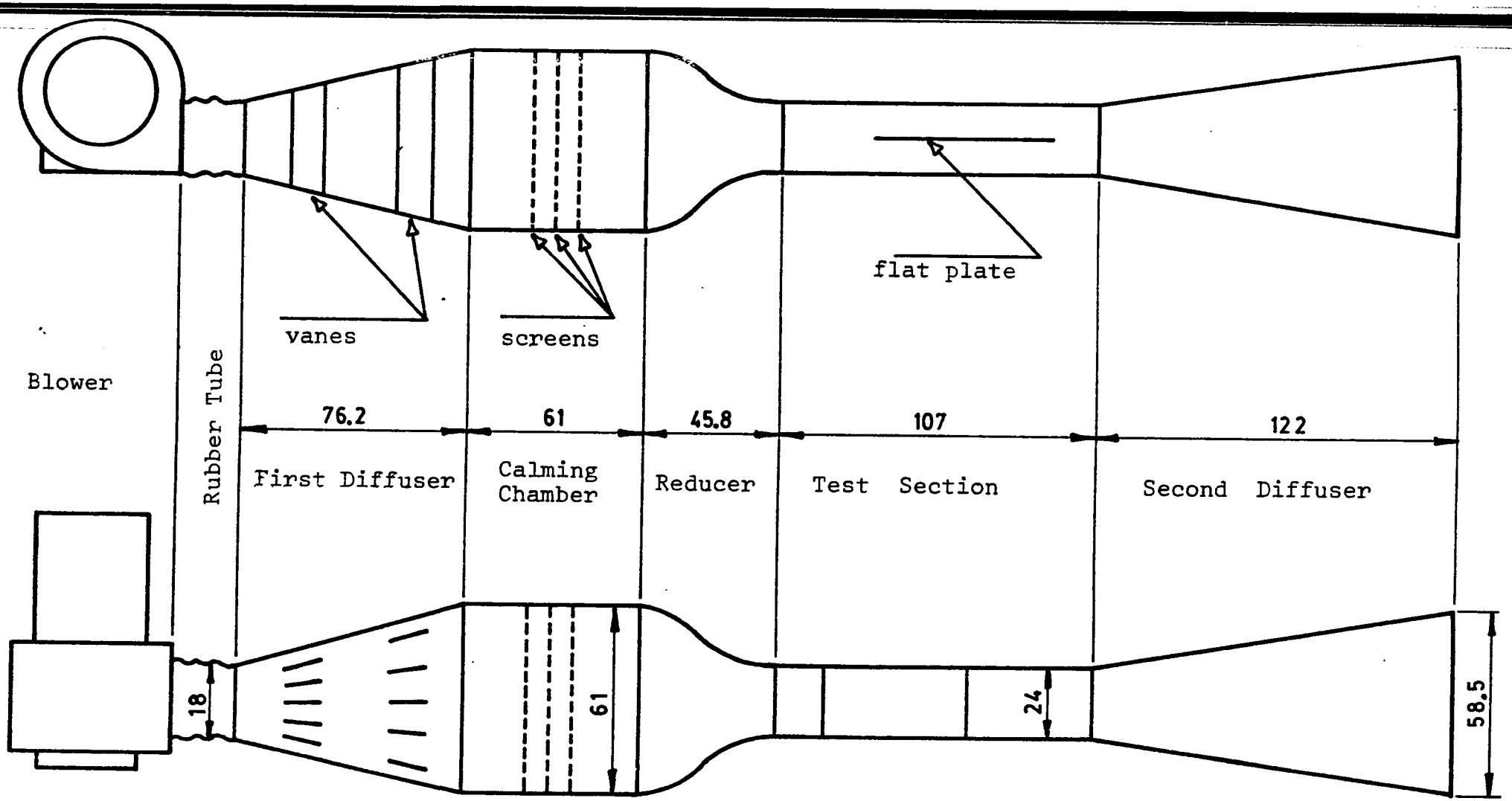

SCALE 1:20

ALL DIMENSIONS IN CENTIMETERS

Figure 1 FLOW SYSTEM

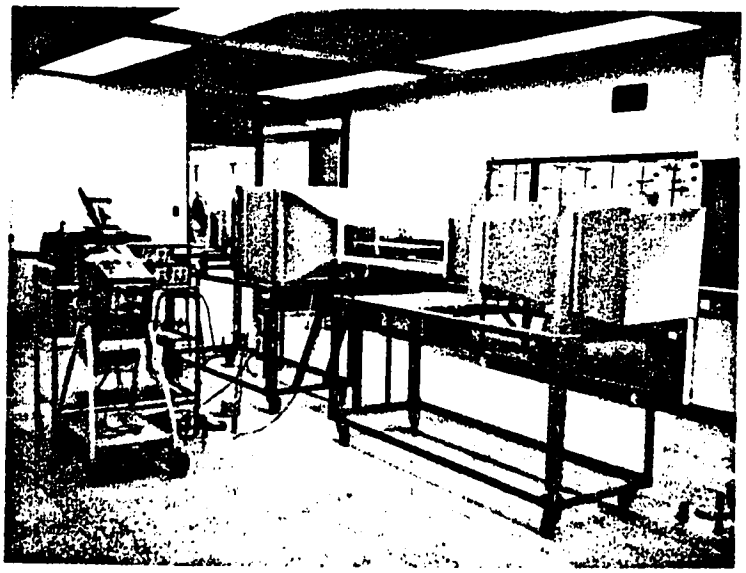

Figure 2. Photograph of Wind Tunnel.

3. Calming Chamber

The settling chamber is a cubic box 61 cm high. Turbulence level control is provided by three fine wire screens fitted inside the chamber and 10 cm apart.

4. Reducer

The reducer is 45.8 cm long with all four sides identical and S-shaped. The curvature of the sides with the inflection point located midway on the reducer axis aids in the smooth acceleration and delivery of the flow to the test section. The reducer aspect ratio is 6.4:1.

5. Test Section

The test section is 107 cm long with a square cross section 24 cm high. It is outfitted with a side door and its roof consists of removable plates 7.6 cm wide each, providing access to the interior of the test section. A sharp-edged flat plexiglass plate 61 cm long and 24 cm wide is fitted inside the test section 12.7 cm below the roof and 15.2 cm from the entrance.

6. Second Diffuser

The second diffuser is 122 cm long. Its square inlet and outlet have heights of 24 cm and 58.5 cm, respectively. Its angle of divergence is 8 degrees and the aspect ratio is 1:5.9.

MEASURING EQUIPMENT

1. Hot-Wire Equipment

The hot-wire equipment used in this study is a single channel anemometer (DISA 55M system) with a constant temperature

standard bridge (type 55M10). The wire probe used (type 55P05) has a resistance of 3.36 ohms and was operated at a constant overheat ratio of 1.13. The manual drive traversing mechanism (type 55H144) was mounted on a steel block which has the same width as the roof plates for the test section. This facilitated the movement of the whole traversing mechanism from one location to another on the test section. Figure 3 shows the details of the probe-traversing-mechanism system. For all of the experimental tests of wall turbulence, the probe wire mounting prongs were resting on the surface of the flat plate in a position that the wire is perpendicular to the direction of the flow and parallel to the plate surface. Therefore, the clearance between the wire and the plate surface can be estimated to be equal to the radius of the probe prong. This was estimated to be 0.13 mm. Figure 4 shows a magnified sketch of the probe-plate contact point.

The anemometer system was tuned and adjusted according to the procedures described in the DISA catalogue. No calibration was required since measurements were made on the frequency rather than on the magnitude of the turbulent signal.

2. Recording Equipment

A Tektronics oscilloscope (type 564B) with storage facility was connected to the anemometer. The scope is outfitted with a polaroid camera to photograph the stored anemometer signals.

3. Velocity Measuring Equipment

The free stream velocity was measured by a pitot-static tube connected to an inclined manometer. The p.s. tube

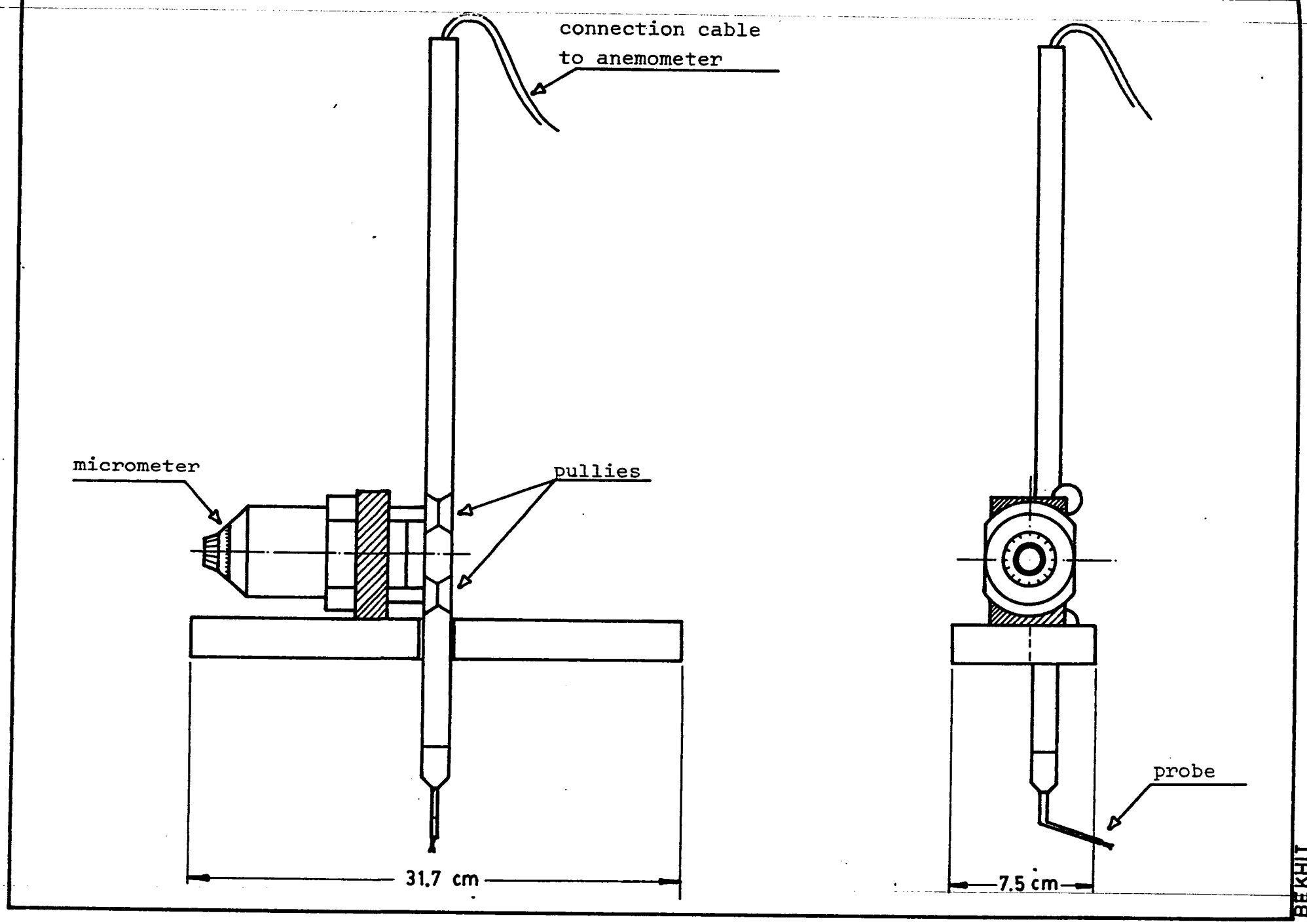

Figure 3 Probe-Traversing-Mechanism System

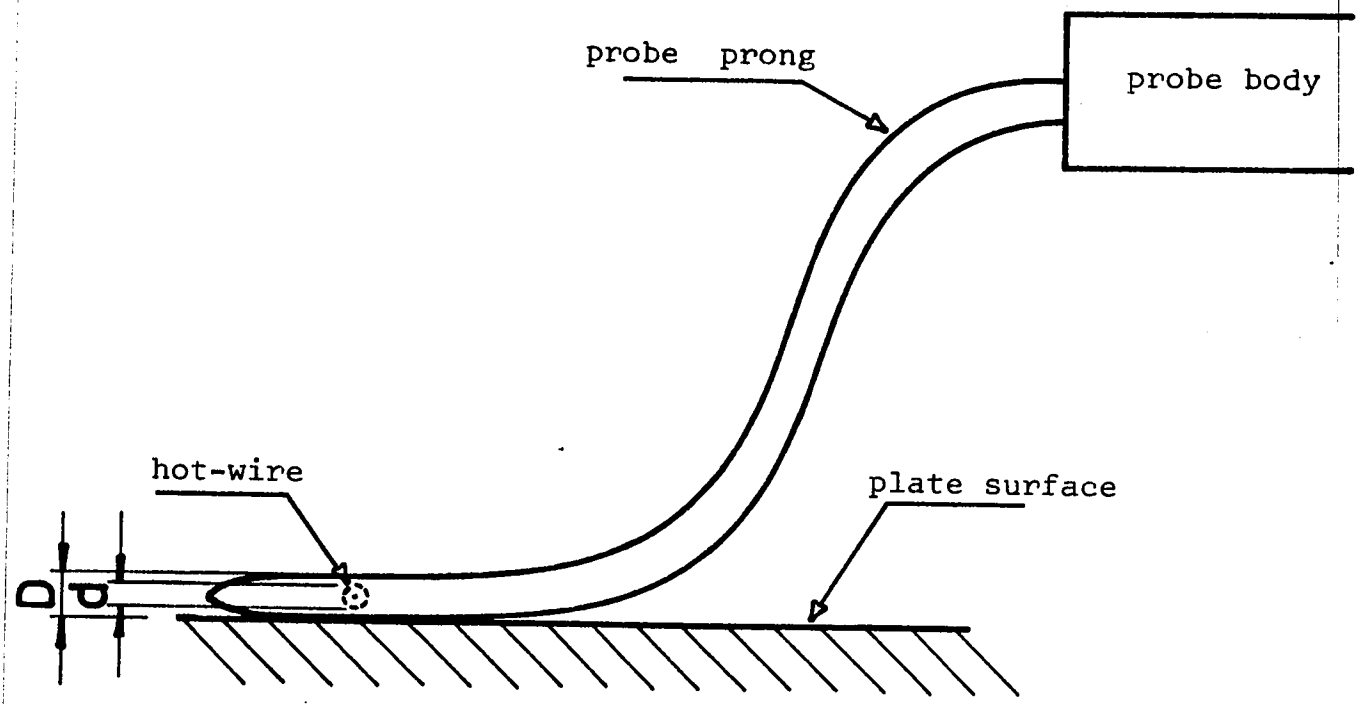

D : probe prong diameter
d : wire diameter

Figure 4 Probe-Plate Contact Point

head was positioned 5 cm above the plate, midway between the sides of the test section and parallel with the flow. Dynamic pressure drop measurements were obtained from two pin-holes drilled in the roof of the test section 15.3 cm apart and connected to an inclined manometer.

PROCEDURES

1. Test Runs

Two experimental runs were conducted in the following manner:

a. The probe was placed in a position over the plate surface and at a certain distance x downstream from the leading edge of the plate. Next, the p.s. tube was connected to the manometer which was leveled an zeroed. The p.s. tube was then placed in position in the vicinity of the probe.

b. With the anemometer in the stand-by position, the temperature of the wire was set by means of setting the overheat ratio. The blower was turned on.

c. The flow system was left for a few minutes to attain steady state. The anemometer was switched to operate position.

d. The portion of the turbulence signal displayed on the scope screen was controlled by changing both the time scale and amplification power of the scope till a distinct representative signal was obtained. Two traces were stored and photographed.

e. The time scale was changed to the next higher setting; and two additional traces were stored and photographed.

f. The two manometers readings, the two scope time-scale settings and the ambient temperature and pressure were recorded. The anemometer was switched back to stand-by position.

g. The flowrate was decreased and steps c,d,e and f were repeated.

h. After several reductions of the flowrate, the signals obtained displayed no fluctuating character. Each run was concluded at this laminar condition.

i. The second run was conducted following the same previous procedure but for a different x position of the probe.

2. Data and Data Treatment

The velocity measured by the p.s. tube can be expressed by the equation

$$u = c\sqrt{2g(P_a - P_d)/\rho_a} = c\sqrt{2g\Delta h\rho_w/\rho_a} \qquad (33)$$

where c is a design factor which is equal to 0.98 for a well designed, average performance tube. At the prevailing ambient temperature of 23°C and pressure of 76 cm-Hg, the following quantities are estimated to be

density of water (ρ_w) = 0.996 Kg/liter
density of air (ρ_a) = 1.19 gm/liter
kinematic viscosity of air (ν_a) = 0.151 cm^2/sec

Thus,

$$u = 1255.2\sqrt{\Delta h} \qquad (34)$$

where Δh is the manometer reading in centimeters of water and u is the velocity in cm/sec.

Sample photographed signals are shown in Figure 5. The average frequency $\bar{s}$ of the signal is obtained by dividing the number of cycles that occurred during a certain interval of time by the time increment. The duration of the

a. Signal obtained at $x = 28$ cm at $Re_x = 1.57 \times 10^5$ and time scale = 2 m.s./div.

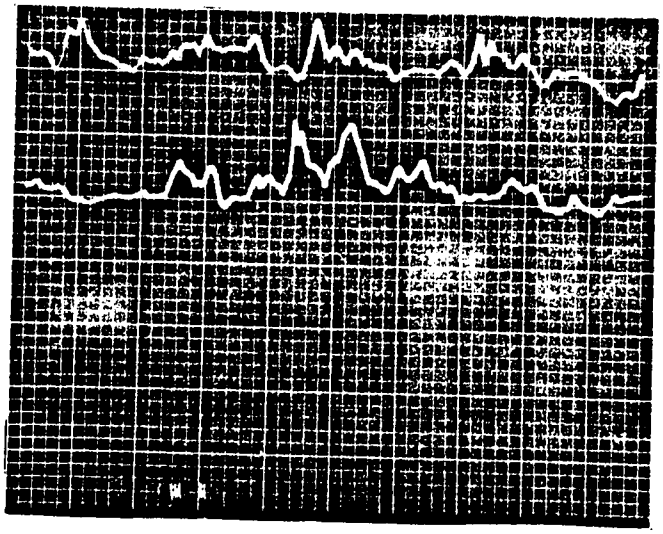

b. same signal in a but with time scale = 5 m.s./div.

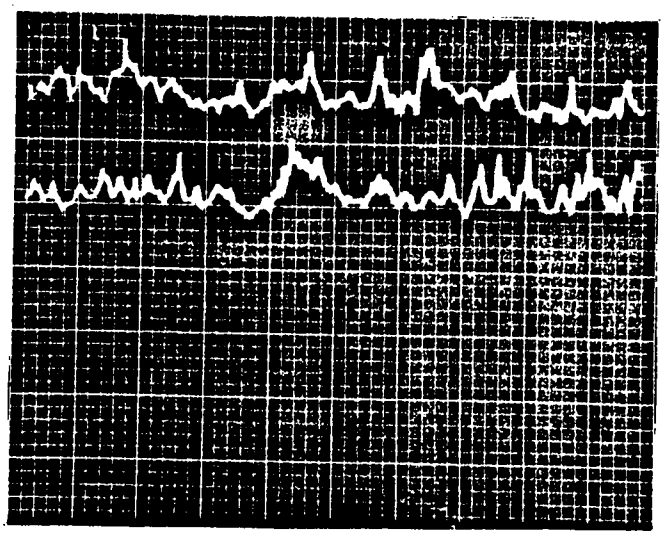

c. signal obtained at $x = 28$ cm at $Re_x = 1.9 \times 10^4$ with time scale = 100 m.s./div.

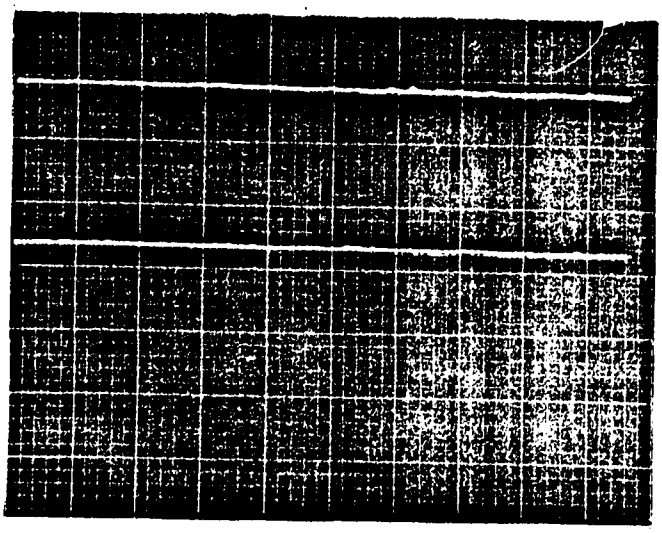

Figure 5 Sample Photographed Signals

stored signal is determined from the time scale setting. The number of cycles, however, is determined by a simple visual technique. Figure 6 shows how a typical signal is interpreted. A complete cycle is construed whenever a major variation in the amplitude of the signal is encountered. This variation might not necessarily be sharp and distinct, but, as was normally encountered, could include minor fluctuations; however the overall trend of an increase followed by a decrease in the amplitude should be observed. The raw and calculated data are shown in tables (1) and (2).

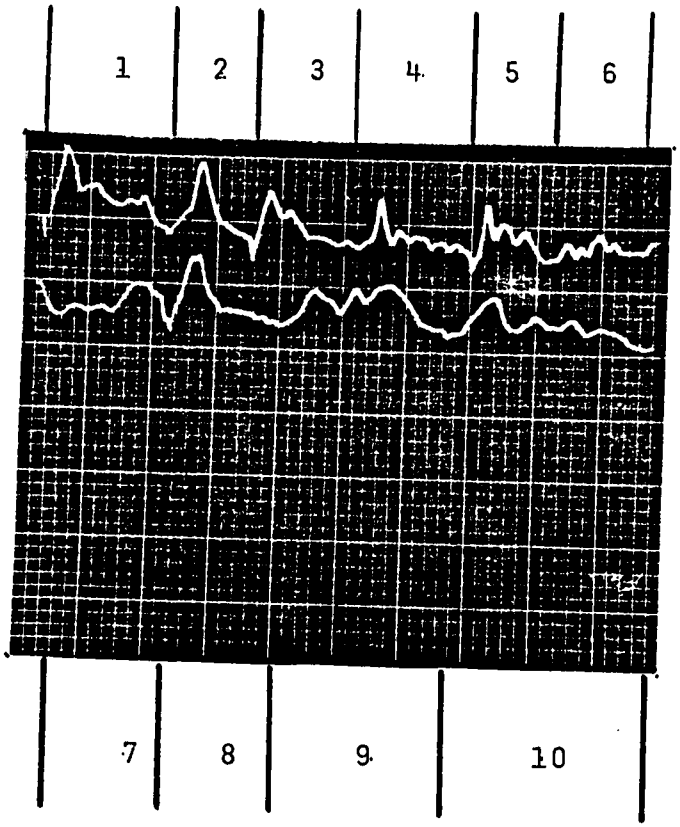

Figure 6 Interpretation of a typical signal. The numbers correspond to individual segments of the signal considered to reflect complete cycles.

TABLE I Raw and Calculated Data for Test Run # 1

x = 53 cm P = 76 cm-Hg
over heat ratio = 1.13 T = 23°C
probe type 55P05

time scale m.s./div.	Δh:p.s. tube cm-H_2O	Re_x x10^{-4}	total time m.s.	Nº of cycles	$(1/\bar{s})$ m.s.	ΔP mm-H_2O
2	0.70	37.0	40	11	3.64	0.31
5	==	==	100	20	5.00	==
2	0.64	35.5	40	9	4.44	0.25
5	==	==	100	19	5.26	==
2	0.56	33.0	40	8	5.00	0.23
5	==	==	100	17	5.88	==
2	0.48	31.0	40	6	6.67	0.19
5	==	==	100	17	5.88	==
5	0.39	28.0	100	13	7.69	0.18
10	==	==	200	20	10.00	==
5	0.32	25.0	100	11	9.09	0.15
10	==	==	200	22	9.09	==
5	0.24	22.0	100	9	11.11	0.13
10	==	==	200	16	12.50	==
10	0.17	18.0	200	12	16.67	0.11
20	==	==	400	16	25.00	==
10	0.13	16.0	200	8	25.00	0.08
20	==	==	400	14	28.57	==
20	0.10	14.0	400	10	40.00	0.05
50	==	==	1000	15	66.67	==
50	0.07	11.5	1000	13	76.92	0.04
100	==	==	2000	15	133.33	==

TABLE I - contd.

time scale m.s./div.	Δh:p.s. tube cm-H_2O	Re_x x10^{-4}	total time m.s.	Nº of cycles	$(1/\bar{s})$ m.s.	ΔP mm-H_2O
50	0.05	10.0	1000	9	111.11	0.03
100	==	==	2000	16	125.00	==
100	0.03	8.2	2000	11	181.82	0.01
200	==	==	4000	13	307.69	==
1000	0.02	6.0	20000	0	∞	

TABLE II Raw and Calculated Data for Test Run # 2

x = 28 cm P = 76 cm-Hg
over heat ratio = 1.13 T = 23°C
probe type 55P05

time scale m.s./div.	Δh:p.s. tube cm-H_2O	Re_x x10^{-4}	total time m.s.	N# of cycles	$(1/\bar{s})$ m.s.
1	0.70	20.0	20	10	2.0
2	==	==	40	19	2.1
2	0.46	15.7	40	10	4.0
5	==	==	100	20	5.0
5	0.24	11.4	100	12	8.3
5	==	==	100	13	7.7
10	0.17	9.4	200	19	10.5
10	==	==	200	13	15.4
20	0.13	8.3	400	10	40.0
20	==	==	400	14	28.6
50	0.11	7.9	1000	29	34.5
50	==	==	1000	26	38.5
50	0.10	7.4	1000	29	34.5
10	==	==	200	2	100.0
50	0.08	6.4	1000	22	45.5
10	==	==	200	3	66.7
20	0.05	5.2	400	7	57.1
10	==	==	200	4	50.0
100	0.03	3.7	2000	10	200.0
500	==	==	10000	0	∞

RESULTS, DISCUSSION & CONCLUSIONS

BOUNDARY LAYER MEASUREMENTS

The signals obtained from the hot-wire anemometer provide the investigator with a record of the various events taking place within the wall region. The photograph shown in Figure 5-a reflects the unsteady fluctuating nature of the flow near the wall. Both major and minor fluctuations are observed to occur. The major peaks are attributed to the direct passage of fluid elements by the hot wire causing a sharp change in the rate of heat transfer. Other minute fluctuations are caused by the various types of disturbances taking place in the vicinity of the wire and yet still sensed by it. This crude classification of the signal features is further refined when another trace of the same signal is taken for a greater oscilloscope time scale. This causes the whole signal to be compressed, with the major peaks becoming more distinct and the secondary effects becoming less noticable as shown in Figure 5-b. Figure 5-c shows a signal which displays no fluctuating character, regardless of the time scale, which indicates that the flow is laminar. This visual analysis proved to be consistent throughout the whole experimental tests. For identical flow conditions, visual analysis of the various signals obtained for different time scale settings gave very close results.

The experiments of Kline et al. (11) revealed, among other results, that the magnitude and type of pressure gradient greatly affects the burst frequency. It was shown that favorable pressure gradients promote stability of the flow and hence reduce the burst rate. They reported relaminarization of the flow when the dimensionless pressure gradient

parameter K

$$K = -\nu/(\rho u_\infty^3) \quad dP/dx \tag{35}$$

exceeded 3.7×10^{-6}. On the other hand, adverse pressure gradients tend to enhance instability of the flow by the greater mixing effects associated with them. Increase in the burst frequency manifests this effect. However, Kline et al. concluded that for values of K less than 5×10^{-7} the effects of pressure gradient on the burst frequency are negligible. Figure 7 shows a plot of K versus Re_x for test run # 1 (x=53 cm). It is observed that the favorable pressure gradient values are far below the lowest limit put by Kline et al.

Figure 8 shows a plot of the mean burst period ($1/\bar{s}$) for both test runs versus Re_x

$$Re_x = u_\infty x/\nu$$

where x is the probe displacement from the leading edge of the plate and u_∞ is the free stream velocity. The burst period is seen to increase logarithmicly as the flow changes from fully turbulent to transitional and laminar conditions. An approximately constant offset is noticed between the results of the two test runs. The points of transition seem to occur around $Re_x = 7 \times 10^4$ and $Re_x = 4 \times 10^4$ for runs # 1 and 2, respectively.

For an ideal fully developed turbulent boundary layer flow with zero pressure gradient, the friction factor is given by (20)

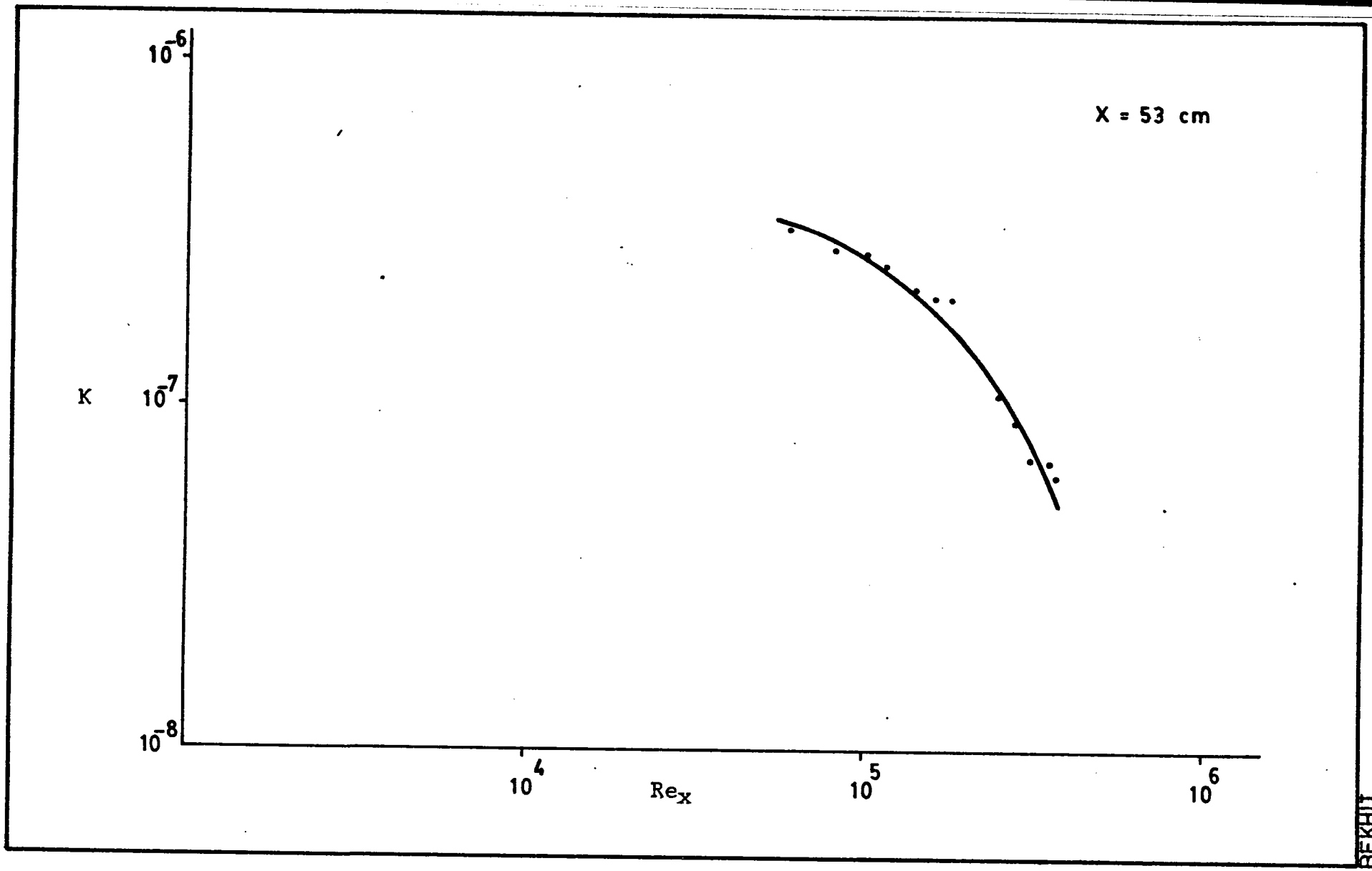

Figure 7 Normalized Pressure Gradient Parameter K vs. Boundary Layer Reynolds Number Re_x for Test Run # 1

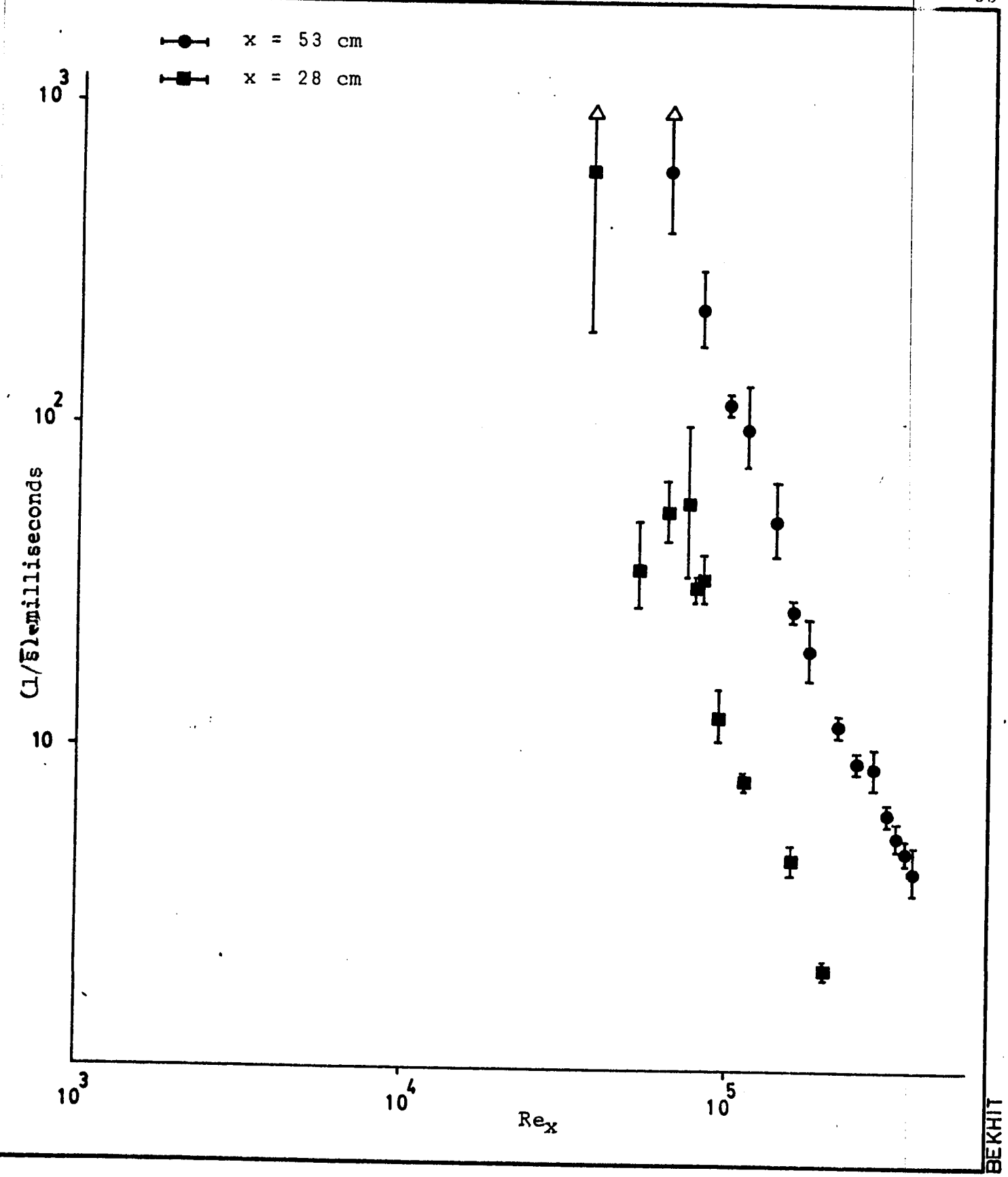

Figure 8 Mean Burst Period vs. Re_x for Test Runs # 1 and 2

$$f_x = 0.059\ Re_x^{-0.2} \tag{37}$$

In such a situation, the dimensionless mean burst period at the wall is predicted to be

$$(1/\bar{s}^+) = u^* \sqrt{1/(\bar{s}\nu)} = U_i/u^*$$

$$= \sqrt{2/f_x} \tag{38}$$

where U_i is set equal to u_∞. Introducing equation (37), equation (38) is rewritten

$$(1/\bar{s}) = 1149\ x^2/\ (\nu\ Re_x^{1.6}) \tag{39}$$

This theoretical curve for fully turbulent boundary layer flow is compared with the data of the two runs in Figures 9 and 10. Equation (39) is seen to follow the data trend in the fully turbulent region ($Re_x > 2 \times 10^5$) but lies above the data by a factor of about four. The primary reason for this offset is that the theory applies to wall measurements while the data was taken at a point off the wall. To see this point, Figure 11-b, obtained from private communication with Dr. L.C. Thomas, is to be examined. This figure is a summary of some of the most important literature data. It is observed that off-wall measurments are genarally lower than wall measurements. The mean value for $(1/\bar{s}^+)$, defined by equation (38), is estimated to be 20 for wall data, while the lowest value for off-wall data is 10. This indicates that the lowest values obtained from experiment for the burst period $(1/\bar{s})$ measured away from the wall are one fourth of the wall measurements. This correlation for off-wall data is represented by the dashed lines in Figures 9 and 10. It is to be recalled at this point that the friction factor corre-

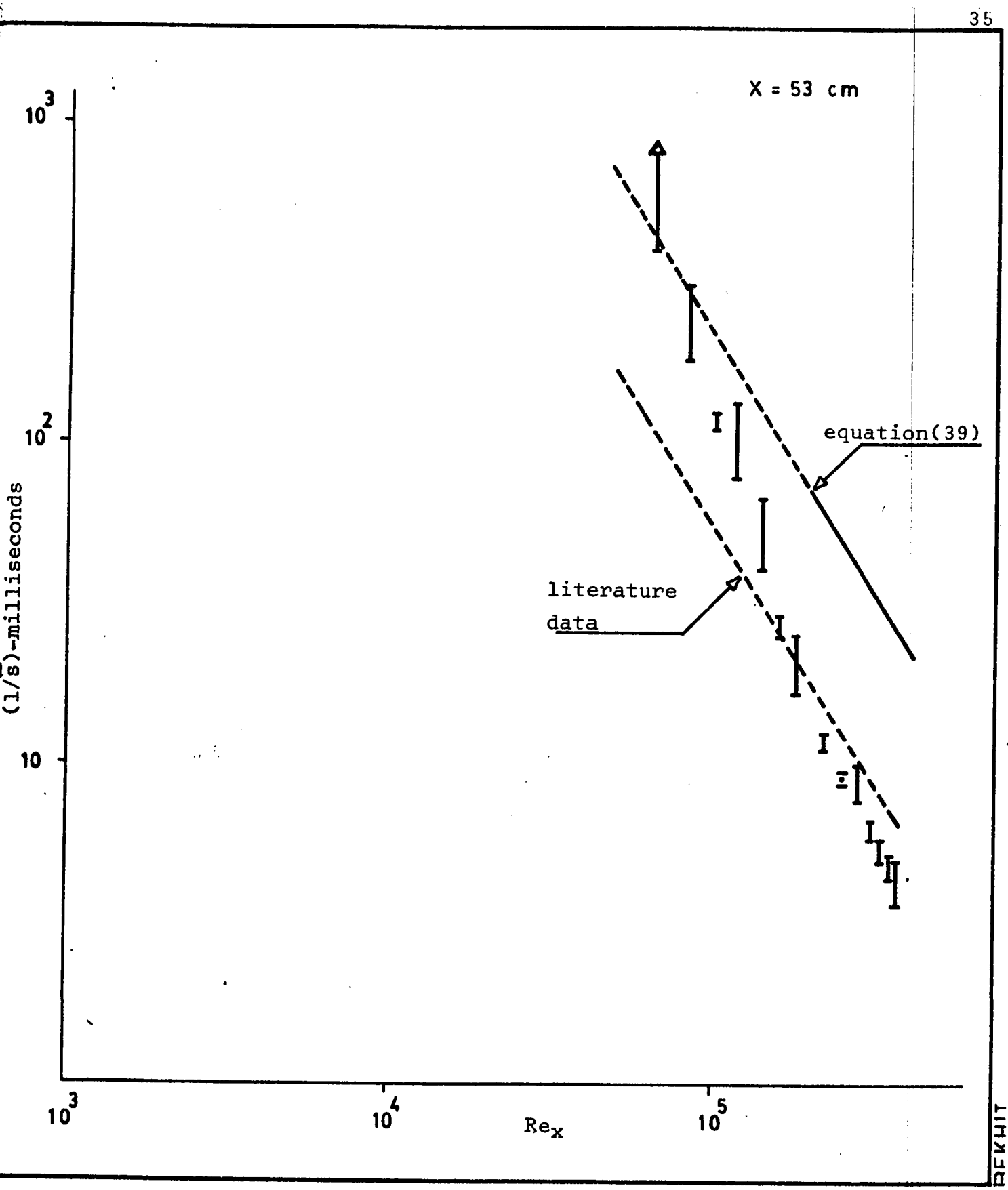

Figure 9 Comparison of Mean Burst Period of Test Run # 1 with Theory and Literature Data

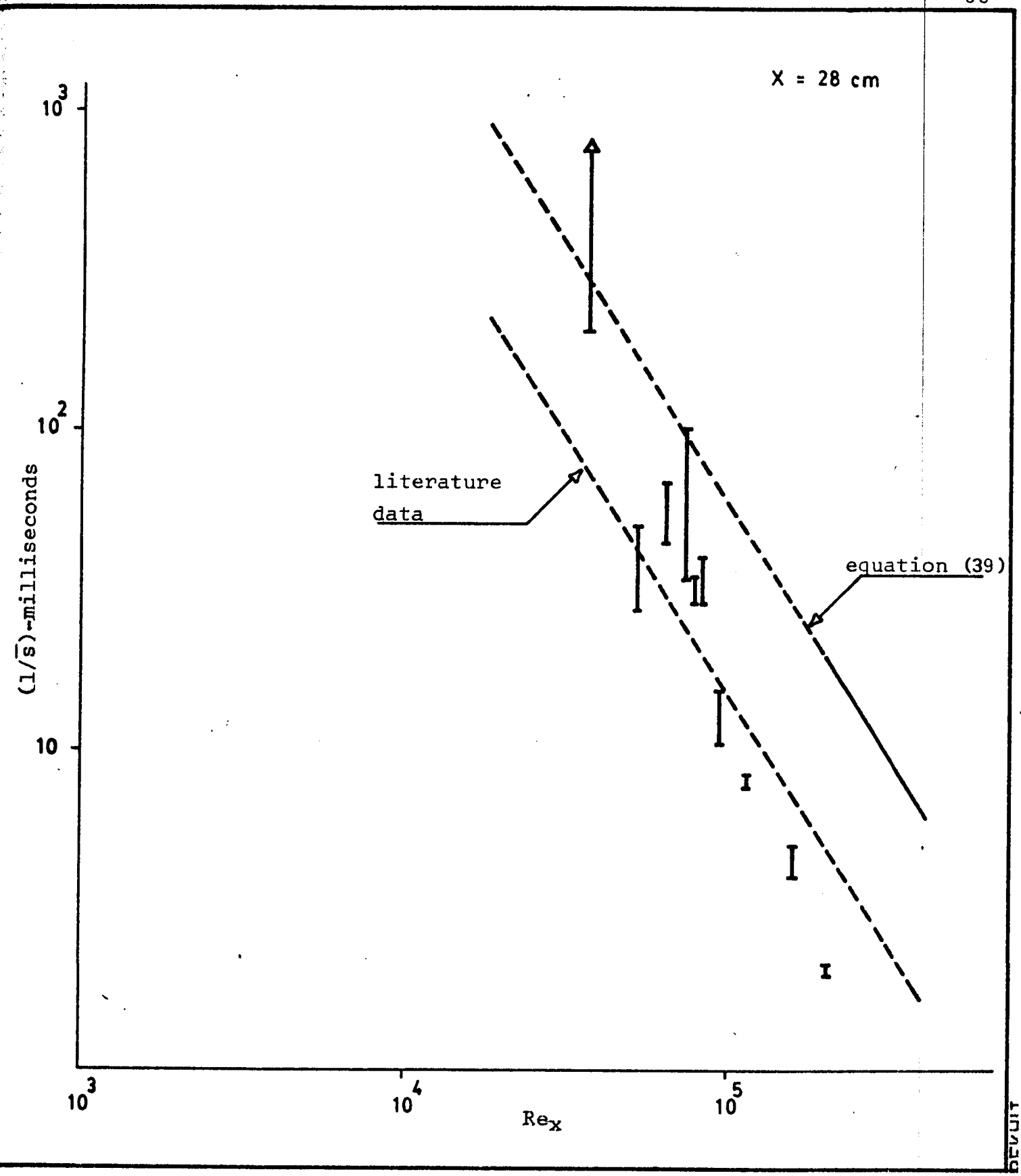

Figure 10 Comparison of Mean Burst Period of Test Run # 2 with Theory and Literature Data

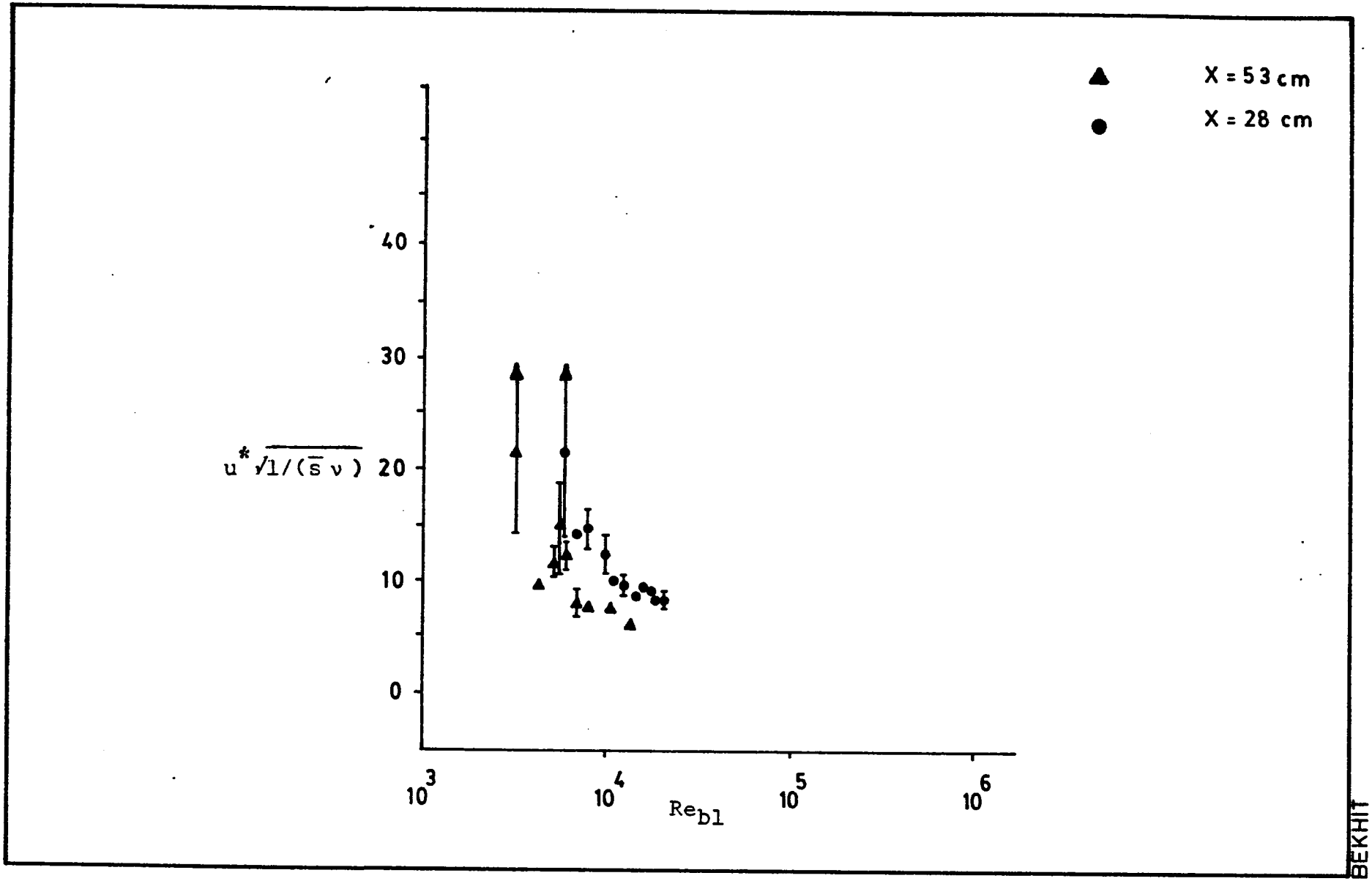

Figure 11-a Summary of data

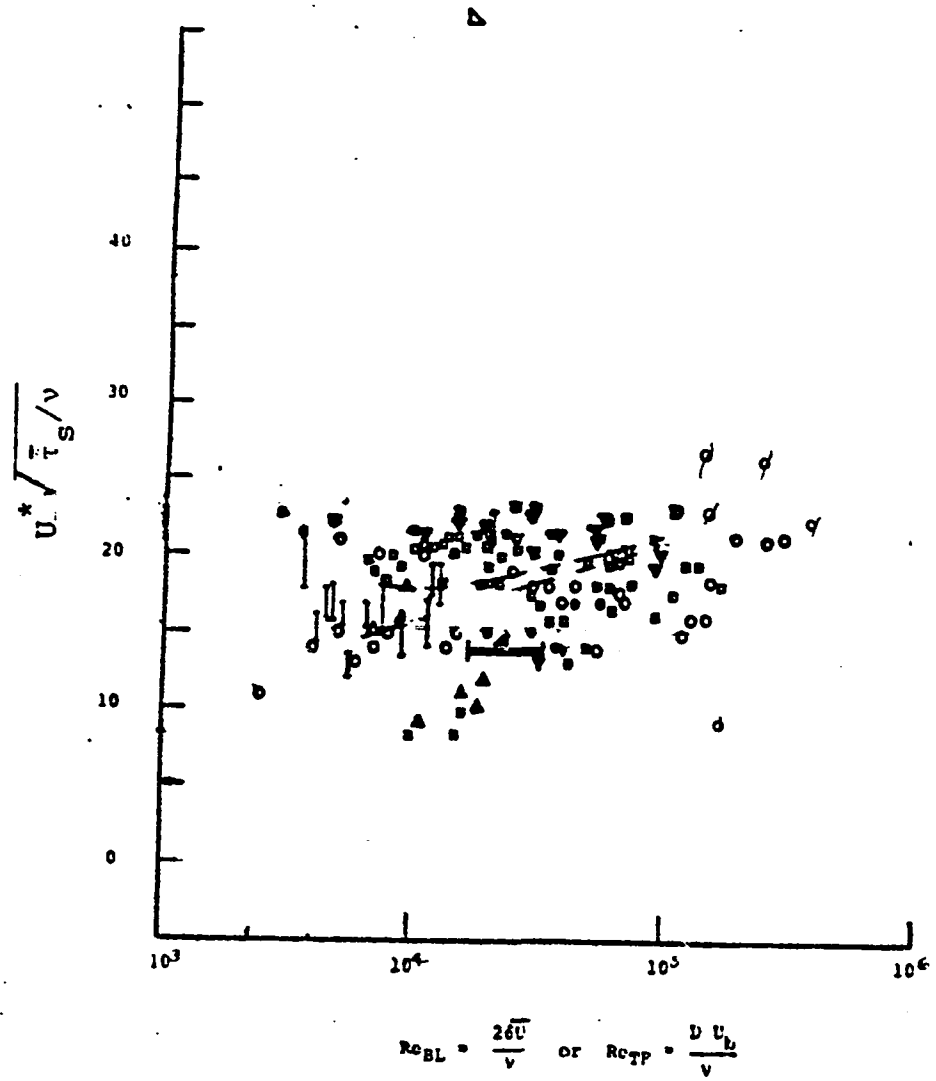

Figure 11b.

SYMBOL	TYPE FLOW	FLUID	MEASURMENT LOCATION	TECHNIQUE	REFERENCE
⟝	BL	Water	y^+=15	Visualization	Schraub,Kline-1965
◢	BL	Water	y^+=15	Visualization	Runstadler et al.-1963
●	BL	Water	y^+>o	Visualization	Corino,Brodkey-1969
■	BL	Air	y^+>o	Anemometry	Rao et al.-1969
▲	BL	Air	y^+>o	Anemometry	Kim et al.-1968
▼	BL	Air	Wall	Anemometry	Laufer,Badri Narayan-1971
◣	BL	Air	y^+>o	Anemometry	Tu,Wilmarth-1961
■	TF	Air	Wall	Anemometry	Meek,Baer-1968
▲	TF	Air	y^+=2	Anemometry	Meek,Baer-1968
◣	TF	*	Wall	Electro-chemical	Mitchel,Hanratty-1965
▼	TF	Tetra-line	Wall	Anemometry	Meek,Baer-1968
o	TF	Air	Wall	Pressure Transducer	Meek,Baer-1968
I	TF	Water NACL	Wall	Anemometry	Thomas,Greene-1971

* Aqueous solution of Sodium Hydroxide and Potassium ferri- and ferrocyanides.

lation given by equation (37) applies only to the fully turbulent flow region. This makes equation (39) invalid for comparison for $Re_x < 2 \times 10^5$.

In order to present the results of this study on Figure 11-b, the boundary layer Reynolds number, defined by

$$Re_{bl} = 2\delta\bar{U}/\nu \tag{40}$$

where δ is the boundary layer thickness and $\bar{U}$ is the flow mean velocity, should be calculated. Re_{bl} is related to Re_x by the following (20)

$$Re_{bl} = 0.763\ Re_x^{0.8} \tag{41}$$

Plotting our results (Figure 11-a) on Figure 11-b reveals that they lie well within the general range of off-wall literature data. Other observed features are the tendency of our data to fall toward minimum mean values of $u^*\sqrt{1/(\bar{s}\nu)} \approx 8.5$ and 7.5 for $Re_{bl} > 10^4$. As Re_{bl} decreases in the transitional turbulent region, $u^*\sqrt{1/(\bar{s}\nu)}$ is seen to increase dramatically toward infinity as laminar conditions are approached. Transition from laminar to turbulent flow conditions occurs within $3000 < Re_{bl} < 5000$. Strictly speaking, equation (41) applies for fully turbulent conditions. However, in order to illustrate the behaviour of $u^*\sqrt{1/(\bar{s}\nu)}$ in the transition region, this equation is utilized for the entire Reynolds number range.

CONCLUSIONS

The survey of literature led to the following conclusions:

1. Turbulence exists in the so-called laminar sublayer of turbulent flow fields with varying intensities. This wall turbulence arises from the interaction of the wall layers with the core of the flow through various dependent motions which manifest themselves by the observed burst phenomena.

2. The burst process enhances the mass and energy transfer rates that take place within the wall region through its mixing effects.

3. The proposed models provided solutions which are closer to the experimental revelations and involve less empiricism than the classical approach to turbulence.

4. Very few measurements have been previously obtained for transitional turbulent flow fields.

Wall turbulence measurements taken in a medium sized wind tunnel that has been designed and constructed for this purpose led to the following conclusions:

5. The burst frequency data taken in the fully turbulent region of $Re_x > 2 \times 10^5$ is in basic agreement with off-wall literature data in the same region.

6. The mean burst period ($1/\bar{s}$) increases with decrease in Re_x in the region of transition from turbulent to laminar conditions.

7. The probe location above the wall lowers the mean burst period ($1/\bar{s}$). In terms of ($1/\bar{s}$), this means that off-wall data lies below on-wall data and theory by a factor of at most four.

8. These results are significant due to the lack of experimental data for transitional turbulent flows. This study is unique from the stand point of investigating the whole range of boundary layer from laminar to fully turbulent.

RECOMMENDATIONS FOR FURTHER WORK

I recommend that the following steps should be undertaken in any further work which involves the same area of research investigated in this study:

1. Use of electronic devices for data collection such as autocorrelators, pressure transducers, etc.

2. Use of flush-mounted anemometer probes and pressure sensors.

The following are problems that could be investigated using the wind tunnel:

3. Study of transitional turbulent flow for the case where the flow develops from laminar to fully turbulent conditions as it travels over the flat plate.

4. Study of the burst phenomena in a solid-gas mass transfer system.

NOMENCLATURE

b	constant
C_i	initial concentration
C_o	equilibrium concentration
c	instantaneous concentration
D	diffusivity coefficient
F	burst rate per unit of span
F^+	normalized burst rate per unit of span
f	Fanning friction factor
f_x	boundary layer friction factor
$f(t)$	time-dependent friction factor
Δh	manometer reading
K	dimensionless pressure gradient parameter
P	pressure
$\overline{P}$	mean pressure
P_d	dynamic pressure
P_s	static pressure
R	instantaneous mass transfer rate
$\overline{R}$	average mass transfer rate
Re	Reynolds number
Re_{bl}	boundary layer thickness Reynolds number
Re_x	boundary layer Reynolds number
s	frequency of renewal
$\overline{s}$	mean frequency of renewal
s^+	dimensionless frequency of renewal
$s(t)$	time-dependent frequency of renewal
$\overline{U}$	mean flow velocity
U_b	bulk flow velocity
Ui	initial velocity
u	instantaneous velocity
$\overline{u}$	time-averaged velocity

u^+	dimensionless velocity
u^*	friction velocity
u_∞	free stream velocity
v	instantaneous y-component velocity
w	channel width
x	distance in main direction of flow measured from leading edge of plate
y	distance transverse to main direction of flow normal to wall
y^+	dimensionless distance in y-coordinate
δ	boundary layer thickness
μ	fluid viscosity
ν	fluid kinematic viscosity
ϕ	statistical age distribution function
ρ	fluid density
ρ_a	density of air
ρ_w	density of water
θ	time from first instant of renewal
τ_o	wall shear stress
κ	constant

REFERENCES

1) Fage, A. & Townend, H.C.H.; 1932 Proc. Roy. Soc. A 135, 656.

2) Lin, C.S., Moulton, R.W. & Putnam, G.L.; 1953 Ind. Engng. Chem. 45,636.

3) Danckwerts, P.V.; I & EC, Vol. 43, 1951, p. 1460

4) Danckwerts, P.V.; A.I.Ch. E.J., 1,456 (1955).

5) Toor, H.L. & Marchello; J.M., A.I. Ch. E.J., 4, 97 (1958).

6) Davidson, J.F.; Trans. Inst. Ch. Engrs., 37, 131(1959).

7) Higbie, R.; Tran. A. Inst. Ch. Engrs., 31, 365(1935).

8) Whitman, W.G.; Chem. Met. Eng., 24,146(1923).

9) Hanratty, T.J.; A.I. Ch. E.J., Vol. 2, 1956, p.359.

10) Einstein, H.A. & Li, H.; ASCE Journal, Eng. Mech. Div., Vol. 82, Nº E.M.1, 1956.

11) Kline, S.J., Reynolds, W.C., Schraub, F.A. & Runstadler, P.W.; J. Fluid Mech., 30, p.741(1967).

12) Corino, E.R. & Brodkey, R.S.; J. Fluid Mech., 37, 1(1969).

13) Meek, R.L. & Baer A.D.; A.I. Ch. E.J., 16, 841(1970a).

14) Thomas, L.C. & Kakarala, C.R.; J. App. Mech., Vol. 43, Trans. ASME, Vol. 98, E (1976).

15) Thomas, L.C. & Min, J.; J. App. Mech., Trans. ASME, p. 559, December (1976).

16) Thomas, L.C.; J. Heat Transfer, Trans. ASME, Vol. 92, p. 565, c(1970).

17) Rao, K.N., et. al.; J. Fluid. Mech., 48, part. 2, p. 339 (1971).

18) Strickland, J.H. & Simpson, R.L.; Tech. Report. WT-2, Southern Methodist University, August (1973).

19) Kays, W.M. & Moretti,P.M.1965 Int.J.H.&M.Trans.8,1187.

20) Davis, J.T. (1972). "Trubulence Phenomena". Academic press, New York.